Gyroscopically Stabilized Quantum Spin Rotors

Vanessa Wachter,[1,2] Silvia Viola Kusminskiy,[2,3] Gabriel Hétet,[4] and Benjamin A. Stickler[1]
[1]Institute for Complex Quantum Systems and Center for Integrated Quantum Science and Technology, Ulm University, Albert-Einstein-Allee 11, 89069 Ulm, Germany
[2]Institute for Theoretical Solid State Physics, RWTH Aachen University, 52074 Aachen, Germany
[3]Max Planck Institute for the Science of Light, Staudtstraße 2, 91058 Erlangen, Germany
[4]Laboratoire de Physique de l'École Normale Supérieure, ENS, PSL, CNRS, Sorbonne Université, Université de Paris, 24 rue Lhomond, 75005 Paris, France

(Received 14 April 2025; accepted 26 January 2026; published 18 February 2026)

Recent experiments demonstrate all-electric spinning of levitated nanodiamonds with embedded nitrogen-vacancy spins. Here, we argue that such gyroscopically stabilized spin rotors offer a promising platform for probing and exploiting quantum spin-rotation coupling of particles hosting a single spin degree of freedom. Specifically, we derive the effective Hamiltonian describing how an embedded spin affects the rotation of rapidly revolving quantum rotors due to the Einstein-de Haas and Barnett effects, which we use to devise experimental protocols for observing this coupling in state-of-the-art experiments. This will open the door for future exploitations of quantum spin rotors for superposition experiments with massive objects.

DOI: 10.1103/zjpt-whpf

The free rotation of a magnetized body can differ significantly from that of the same object if it were nonmagnetic. This, perhaps surprising, discrepancy is due to the fact that magnetic moments carry a spin angular momentum that contributes to the total angular momentum of the magnetized body, as quantified by the material-specific gyromagnetic ratio. Remarkably, it is the *total* angular momentum, i.e., the sum of mechanical and spin angular momentum, that enters the equations of motion of the body [1]. This gives rise to the so-called spin-rotation coupling [2] between rigid-body rotations and magnetic degrees of freedom, as famously witnessed in the Einstein-de Haas and Barnett effects [3–7]. The impact of spin-rotation coupling typically decreases with particle size, while it is still relevant for microscale and nanoscale magnetic objects [8–13].

Nanoscale particles of various shapes and with sizes ranging from hundreds of nanometers to tens of microns can be stably suspended in ultrahigh vacuum using optical, electrical, or magnetic traps [14]. Monitoring and controlling their linear and rotational motion with laser fields enables precision sensing of forces and torques as required for fundamental tests of physics [15,16]. Recent demonstrations of cooling their center-of-mass oscillations [17–20] and their angular librations [21–23] in an optical tweezer into the quantum regime constitute the first steps toward quantum applications of levitated particles. The demonstrated degree of control and readout renders these systems ideal for performing quantum experiments with objects of unrivaled masses [24–29].

Experiments with levitated magnetic objects aim at harnessing their magnetic properties to gain better control over the internal and external degrees of freedom of the nanoparticle [30]. Magnetized particles have been trapped in electric [31,32], magnetic [33–35], optical [36,37], and superconducting traps [38–40], where their center-of-mass and rotational motion can be monitored and manipulated. Various schemes have been devised to control their mechanical motion via driving the internal magnetization field [41–46] or individual magnetic defect centers, such as nitrogen-vacancy (NV) centers [30,47–54]. These schemes promise to enable sensing of magnetic fields and accelerations [9,39,55–57], as well as the creation of massive superpositions [27,58–62], and perhaps even probing the quantumness of gravity [63].

In this Letter, we show how the spin-rotation coupling between a levitated nanoparticle and a single embedded spin degree of freedom can be observed and exploited for quantum experiments. The proposed scheme is based on the recent experimental demonstration of rapid spinning of electrically levitated nanodiamonds with embedded spin degrees of freedom [32,64]. This spinning boosts the spin-rotation coupling while it also gyroscopically stabilizes the nanoparticle orientation in the corotating frame (see Fig. 1), so a combination of magnetostatic fields and microwave pulses then enables controlling the collective motion of hundreds of millions of atoms via a single spin.

Published by the American Physical Society under the terms of the Creative Commons Attribution 4.0 International license. Further distribution of this work must maintain attribution to the author(s) and the published article's title, journal citation, and DOI.

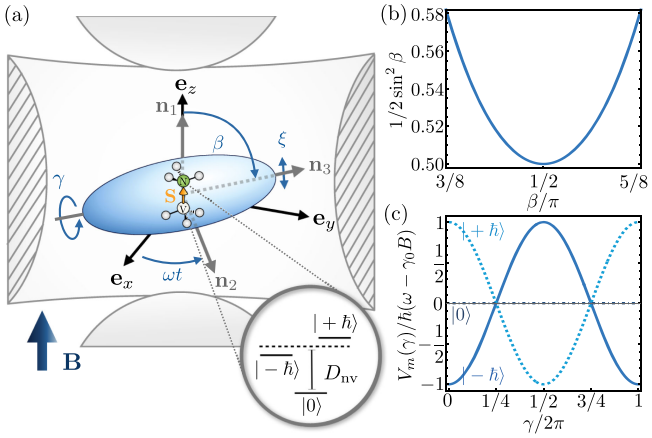


FIG. 1. (a) Charged spheroidal nanodiamond with an embedded nitrogen-vacancy (NV) center is levitated in a Paul trap and revolves rapidly with frequency ω in the symmetry plane of the trap. The major principal axis $\mathbf{n}_1$ of the body is chosen to be aligned with the NV quantization axis so that the NV spin states $|S_1 = \pm\hbar\rangle$ are split by the rotation-induced Barnett field as well as by an applied magnetic field $\mathbf{B}$. The particle rotation induces (b) an effective gyroscopic potential $I\omega^2/2\sin^2\beta$ stabilizing the out-of-plane rotation angle β, up to small librations ξ, while the external magnetic field together with spin-rotation coupling induce (c) a spin state-dependent potential $V_m(\gamma)$ for γ rotations around the body-fixed symmetry axis depending on the spin states $|S_1 = \hbar m\rangle$ with $m \in \{-1, 0, 1\}$.

Specifically, we consider a symmetric nanodiamond with a single embedded NV spin levitated in the presence of an external static magnetic field $\mathbf{B} = B\mathbf{e}_z$, as schematically depicted in Fig. 1. The nanodiamond is approximated as an ellipsoidal rigid rotor with semiaxis lengths $l_1 = l_2 < l_3$ and moments of inertia $I_1 = I_2 = I$ with $I_3 < I$. The nanoparticle orientation $\Omega = (\alpha, \beta, \gamma)$, parametrized by Euler angles in the $z - y' - z''$ convention, specifies the tensor $\mathrm{R}(\Omega)$ which rotates from the lab-frame axis $\mathbf{e}_j$, $j = x, y, z$, to the rotor principal axes $\mathbf{n}_\mu(\Omega) = \mathrm{R}(\Omega)\mathbf{e}_j$, $\mu = 1, 2, 3$. For instance, $\mathbf{n}_1(\Omega) = \mathrm{R}(\Omega)\mathbf{e}_x$, etc.; an explicit expression for $\mathbf{n}_\mu(\Omega)$ is given in Supplemental Material [65]. The inertia tensor depends on the orientation of the particle through $\mathrm{I}(\Omega) = \sum_\mu I_\mu \mathbf{n}_\mu(\Omega) \otimes \mathbf{n}_\mu(\Omega)$. A single NV center with spin-one angular momentum vector operator $\mathbf{S}$ is embedded in the nanodiamond, effectively introducing an internal spin triplet and adding the magnetic dipole moment $\gamma_0\mathbf{S}$ to the particle (with gyromagnetic ratio $\gamma_0 > 0$). The spin angular momentum adds to the mechanical angular momentum to yield the total angular momentum $\mathbf{J}$ of the system. For the spin quantization axis, we choose $\mathbf{n}_1(\Omega)$, effectively breaking the symmetry of the particle shape; the NV zero-field splitting is $D_{\mathrm{nv}} \simeq 2\pi \times 2.87$ GHz. Possible imperfections, such as weak deviations from axial symmetry or small misalignment of the NV axis relative to the principal inertia axis, are analyzed in Supplemental Material [65].

Gyroscopic stabilization is achieved by trapping a charged particle in an azimuthally symmetric quadrupole trap and spinning it with high rotation frequency ω around the lab-frame $\mathbf{e}_z$ axis, as recently realized in two experiments [32,64]. For homogeneously charged particles the electric quadrupole tensor aligns with the inertia tensor, with quadrupole moments $Q_1 = Q_2 = Q$ and $Q_3 > Q$. For vanishing electric dipole moment, the center-of-mass and rotational motion of the particle decouple so that the resulting rotational macromotion potential is determined by the ac voltage U_{ac}, the electrode separation d_0, and the ac frequency ω_{ac} [83]. The spin-rotor Hamiltonian is

$$H = \frac{(\mathbf{J}-\mathbf{S})^2}{2I} + \left(\frac{1}{2I_3} - \frac{1}{2I}\right)(J_3 - S_3)^2 + \frac{D_{\mathrm{nv}}}{\hbar}S_1^2 - \gamma_0 B\left(S_1\sin\beta\cos\gamma - S_2\sin\beta\sin\gamma - S_3\cos\beta\right) + \frac{U_{\mathrm{ac}}^2(Q-Q_3)^2}{16I\omega_{\mathrm{ac}}^2 d_0^4}\sin^2\beta\cos^2\beta. \tag{1}$$

Here, $J_\mu = \mathbf{J}\cdot\mathbf{n}_\mu(\Omega)$ denotes the body-frame component of the total angular momentum vector and likewise for $\mathbf{S}$. The confining quadrupole potential depends only on the polar angle β, implying that the lab-frame angular momentum component $p_\alpha = \mathbf{J}\cdot\mathbf{e}_z$ is conserved. It is thus convenient to transform the spin-rotor state $|\psi\rangle$ to a corotating frame of boosted angular momentum via

$$|\psi\rangle = \exp\left(i\frac{I\omega}{\hbar}\alpha - i\omega t\frac{p_\alpha}{\hbar}\right)|\phi\rangle. \tag{2}$$

This adds the gyroscopic potential $I\omega^2/2\sin^2\beta$ [see Fig. 1(b)] to the quadrupole potential in Eq. (1), effectively confining the particle to the rotation plane $\beta \simeq \pi/2$ with harmonic frequency

$$\omega_\xi = \sqrt{\omega^2 + \frac{U_{\mathrm{ac}}^2(Q-Q_3)^2}{8I^2\omega_{\mathrm{ac}}^2 d_0^4}}. \tag{3}$$

For large rotation rates $\omega_\xi \simeq \omega$ [65], librations out of the rotation plane can be first linearized in $\xi = \pi/2 - \beta$ and then adiabatically eliminated. Specifically, linearization yields

$$H_{\mathrm{rot}} = H_\xi + \frac{p_\gamma^2}{2I_3} + \frac{D_{\mathrm{nv}}}{\hbar}S_1^2 + (\gamma_0 B S_3 - \omega p_\gamma)\xi + (\omega - \gamma_0 B)(S_1\cos\gamma - S_2\sin\gamma), \tag{4}$$

with $p_\gamma = J_3$, $H_\xi = p_\xi^2/2I + I\omega_\xi^2\xi^2/2$, and nondominant contributions to spin-rotation coupling as well as dispersion in the gyroscopic motion being neglected [65]. The fast librations out of the rotation plane can now be eliminated by neglecting transitions between eigenstates $|n\rangle$ of H_ξ in a Born-Oppenheimer approximation [65]. This is achieved

by expanding

$$|\phi\rangle = \sum_{n=0}^{\infty} \exp\left[-\frac{ip_\xi}{\hbar}\frac{\omega p_\gamma - \gamma_0 B S_3}{I\omega^2}\right] e^{-itH_\xi/\hbar}|n,\chi_n\rangle, \tag{5}$$

so that the adiabatic spin-rotor state $|\chi_n\rangle$ evolves according to the Hamiltonian

$$\begin{aligned} H_n = {} & \frac{p_\gamma^2}{2I_{\rm eff}} + \frac{\gamma_0 B}{I\omega} S_3 p_\gamma + \frac{D_{\rm nv}}{2\hbar}(S_1^2 + S_2^2) \\ & + \frac{1}{2}(\omega - \gamma_0 B)[f_n(S_1 - iS_2)e^{-i\gamma} + \text{H.c.}] \\ & + \frac{D_{\rm nv}}{4\hbar}[g_n(S_1 + iS_2)^2 + \text{H.c.}]. \end{aligned} \tag{6}$$

This Hamiltonian describes the coupling between the NV spin and γ rotations with effective inertia $I_{\rm eff} = II_3/(I - I_3)$. The final two terms are the adiabatic potential (or potential energy surface) for fixed libration state $|n\rangle$, containing the magnetic potential as well as spin-rotation coupling and the Barnett effect on the NV zero-field splitting. The adiabatic terms are weighted by the overlap integrals

$$f_n = \langle n| \exp\left(-\frac{ip_\xi}{\hbar}\frac{\hbar(\omega - \gamma_0 B)}{I\omega^2}\right)|n\rangle, \tag{7a}$$

$$g_n = \langle n| \exp\left(-\frac{ip_\xi}{\hbar}\frac{2\hbar\gamma_0 B}{I\omega^2}\right)|n\rangle, \tag{7b}$$

for transitions between displaced and nondisplaced libration states. Note that $f_n \simeq 1$ for $n \ll I^2\omega^4/\hbar^2\gamma_0^2 B^2$ and likewise $g_n \simeq 1$. Given that $\hbar\gamma_0 B/I\omega^2 \ll 1$ for realistic magnetic fields and rotation rates, the Hamiltonian (4) becomes approximately independent of n. Thus, all adiabatic spin-rotor states $|\chi_n\rangle$ evolve according to the same effective Hamiltonian:

$$\begin{aligned} H_{\rm eff} = {} & \frac{p_\gamma^2}{2I_{\rm eff}} + \frac{D_{\rm nv}}{\hbar} S_1^2 + \frac{\gamma_0 B}{\omega}\frac{S_3 p_\gamma}{I} \\ & + (\omega - \gamma_0 B)(S_1 \cos\gamma - S_2 \sin\gamma). \end{aligned} \tag{8}$$

This Hamiltonian is the main result of this Letter and the starting point for the proposals discussed below. It accounts for spin-rotation coupling in three different ways. First, the planar γ rotation occurs with the effective moment of inertia $I_{\rm eff}$ because ξ librations are gyroscopically stabilized and adiabatically eliminated. Second, the rotation rate ω of the particle induces the effective spin-dependent potential in the second line of the Hamiltonian (8). Third, the $\mathbf{B}$ field induces a coupling of the spin to rotations around the symmetry axis of the particle as described by the last term in the first line. Note that this coupling is typically small and will be neglected in the following (see Supplemental Material [65]). Next, we will study the implications of gyroscopic stabilization for the experimental observation of strong spin-rotation coupling.

(a) Barnett splitting—The Hamiltonian shows how the degeneracy of the $|S_1 = \pm\hbar\rangle$ states is lifted by the Barnett effect for $B = 0$. Specifically, neglecting γ rotations by setting $\gamma = 0$ and $p_\gamma = 0$, the $|S_1 = \pm\hbar\rangle$ levels are split by the gyroscopic rotation frequency ω. Note that the resonance frequency is also Doppler shifted by the particle rotation rate since the microwave drive is applied in the lab frame rather than in the rotating frame of the NV center [84–86].

(b) Barnett alignment—The described setup can be used to observe that the Barnett field $-\omega/\gamma_0$ tends to align prolate particles with their own rotation axis [11]. This follows from considering the hard magnet limit $|\omega - \gamma_0 B| \ll D_{\rm nv}$, where the spin is rigidly attached to the body frame $S_1 = \hbar m$ with $m \in \{-1, 0, 1\}$ and $S_2 = S_3 = 0$. Then the adiabatic Hamiltonian (8) implies that the particle revolves according to the spin-dependent potential $V_m(\gamma) = \hbar m(\omega - \gamma_0 B)\cos\gamma$ [see Fig. 1(c)],

$$I_{\rm eff}\ddot{\gamma} = \hbar m(\omega - \gamma_0 B)\sin\gamma. \tag{9}$$

For $B = 0$ and $m = 1$, the rotor tends to orient with $\gamma = \pi$ so that the rotation axis aligns with the spin axis. A finite magnetic field $B > 0$ weakens the impact of the Barnett field and exactly compensates it at $B = \omega/\gamma_0$, where the particle evolves freely in γ, as would be expected for an object carrying no spin degrees of freedom. Experimentally observing the alignment of the particle spin axis with the rotation axis is thus a unique signature of strong spin-rotation coupling in a rotating nanoparticle. It can be observed in state-of-the-art experiments with nanodiamonds spinning in quadrupole ion traps. This is illustrated in Fig. 2(a), which shows the steady-state alignment $\langle\cos\gamma\rangle$ of the NV axis as a function of the rotation rate ω for three different temperatures. Note that a robust implementation in the presence of rotor asymmetries uses nanodiamonds hosting multiple NV centers (see Supplemental Material [65]).

(c) Stabilization of spin superpositions—For moderate magnetic fields, the superposition of the magnetic spin states $|\sigma_x = +1\rangle = (|S_1 = +\hbar\rangle + |S_1 = -\hbar\rangle)/\sqrt{2}$ becomes stabilized when the spin quantization axis lies in the rotation plane. Specifically, for $|\omega - \gamma_0 B| \lesssim D_{\rm nv}$, the nonmagnetic state $|S_1 = 0\rangle$ remains far detuned from the magnetic states $|S_1 = \pm\hbar\rangle$ for all orientations γ. The former can thus be adiabatically eliminated, yielding the spin-rotor Hamiltonian in the magnetic spin subspace

$$H_{\rm mag} = \frac{p_\gamma^2}{2I_{\rm eff}} + \frac{\hbar\delta}{2}(\mathbb{1} + \sigma_x)\sin^2\gamma + \hbar g\sigma_z\cos\gamma. \tag{10}$$

Here, $\delta = (\omega - \gamma_0 B)^2/D_{\rm nv}$, $g = (\omega - \gamma_0 B)$, and σ_z and σ_x are Pauli matrices in the magnetic subspace of the NV spin.

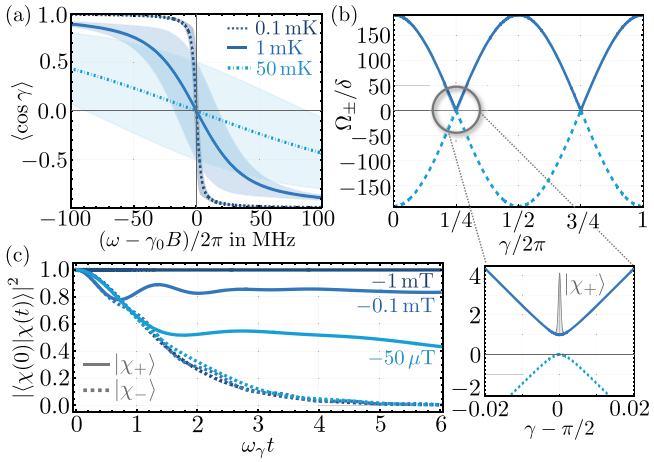


FIG. 2. (a) Steady-state alignment $\langle\cos\gamma\rangle$ as a function of the applied magnetic field. The variance is indicated by the shaded region. (b) Potential energy surfaces Ω_+ (solid) and Ω_- (dashed) for $B=-0.5$ mT and $\omega/2\pi=1$ MHz. The inset shows the avoided crossing around $\gamma=\pi/2$ where the spin-rotor state $|\chi_+\rangle$ can be stably trapped in the $|\sigma_x=+1\rangle$ spin state. (c) Spin transition probability for an initial state in spin $|\sigma_x=+1\rangle$ (solid) and spin $|\sigma_x=-1\rangle$ (dashed) as a function of $\omega_\gamma t$ for different magnetic field strengths. The nanodiamond has an ellipsoidal shape with semiaxes $l_3=200$ nm and $l_1=l_2=0.3l_3$.

In contrast to the hard magnet limit, this Hamiltonian accounts for spin transitions as described by $\delta\neq 0$. Diagonalizing the spin-dependent part of Eq. (10) yields the potential energy surfaces $\hbar\Omega_\pm(\gamma)/2$ for the γ dynamics,

$$\Omega_\pm(\gamma)=\delta\sin^2\gamma\pm\sqrt{\delta^2\sin^4\gamma+4g^2\cos^2\gamma}, \quad (11)$$

as depicted in Fig. 2(b). They exhibit an avoided crossing at $\gamma=\pi/2$ (and $3\pi/2$), in addition to the potential minima at $\gamma=0,\pi$ for $|S_1=\pm\hbar\rangle$ already observed in the hard magnet limit. The energies can be linearized near the avoided crossing yielding $\hbar\Omega_\pm(\gamma)=\pm\hbar\delta/2\pm\hbar g^2(\gamma-\pi/2)^2/\delta$, showing that the spin rotor is harmonically trapped in the spin state $|\sigma_x=+1\rangle$. The ground state of the resulting harmonic potential is stably trapped for $|\delta|\gg|g\sigma_\gamma|$, where $\sigma_\gamma=(\hbar\delta/8I_{\rm eff}g^2)^{1/4}$ is the ground state width in the effective harmonic potential [65]. The state becomes unstable if this condition is violated, as illustrated in Fig. 2(c) for three different magnetic field strengths, or when the spin superposition decoheres.

(d) Spin-controlled quantum interference—For strong magnetic fields, $|\omega-\gamma_0 B|\simeq D_{\rm nv}$, the quantum state of the NV spin can be used to generate and read out superpositions of the angle γ. Specifically, the magnetic state $|S_1=+\hbar\rangle$ can be adiabatically eliminated for small librations around $\gamma\simeq 0$, restricting the spin to the two levels $|\uparrow\rangle=|S_1=-\hbar\rangle$ and $|\downarrow\rangle=|S_1=0\rangle$ with detuning $\Delta=D_{\rm nv}-g$. For small amplitudes and detunings $\langle\gamma^2\rangle\ll|\Delta|/|g|\ll 1$, the two spins are effectively decoupled, and the resulting dispersive spin-rotor Hamiltonian follows as [65]

$$H_{\rm d}=\frac{p_\gamma^2}{2I_{\rm eff}}+\frac{\hbar g}{8}\gamma^2+\frac{\hbar\Delta}{2}\sigma_z+\frac{3\hbar g}{8}\left(1+\frac{4g}{3\Delta}\right)\gamma^2\sigma_z. \quad (12)$$

This dispersive Hamiltonian (12) can be used to create and read out nonclassical states of the rotor with a simplified version of the scheme discussed in Ref. [12]. Specifically, for $\Delta>0$, the spin is initialized in $|\uparrow\rangle$, while the rotor is prepared in a thermal oscillator state $\rho_{\rm th}$ with corresponding frequency $\omega_\gamma=\sqrt{\hbar g(1+g/\Delta)/I_{\rm eff}}$ and temperature T, $\rho=\rho_{\rm th}\otimes|\uparrow\rangle\langle\uparrow|$. The interference protocol is then implemented in three steps [see Fig. 3(a)]: (i) a microwave $\pi/2$-pulse is applied to prepare the spin in a superposition $|\uparrow\rangle\to(|\uparrow\rangle+|\downarrow\rangle)/\sqrt{2}$. The oscillator then evolves for a time τ, during which the branch with spin $|\downarrow\rangle$ becomes squeezed. (ii) At time $t=\tau$, a microwave π-pulse reverses the role of the spin $|\uparrow(\downarrow)\rangle\to|\downarrow(\uparrow)\rangle$, followed by a second evolution over a time τ which now squeezes the thermal oscillator in the second spin branch. (iii) A final $\pi/2$-pulse at $t=2\tau$ closes the interferometer through $|\uparrow(\downarrow)\rangle\to(|\uparrow\rangle\pm|\downarrow\rangle)/\sqrt{2}$, creating a superposition of squeezed states. The microwave pulses are applied in the lab frame and therefore experience a rotational Doppler shift in the NV frame; however, the drive remains resonant throughout the rotation, ensuring coherent spin control during the entire protocol [65]. The evolution of the oscillator during the pulse is negligible as the pulse duration is much shorter than the timescale of its dynamics. The probability of measuring spin $|\uparrow(\downarrow)\rangle$ after the interferometer sequence is $P_{\uparrow\downarrow}=1/2\pm\exp(-2\tau/T_2)\sqrt{|\lambda_\tau|}\cos[\arg(\lambda_\tau)/2]/2$, with the Hahn-echo spin dephasing time T_2 and the time-dependent complex number λ_τ [65]. For small temperatures $T\ll\hbar\omega_\gamma/k_{\rm B}$, with the Boltzmann constant $k_{\rm B}$, it is determined by

$$\frac{1}{\lambda_\tau}=1+(1-e^{2i\omega_\gamma\tau})\sinh^2\left(\frac{\sqrt{\hbar}g\tau}{\sqrt{I_{\rm eff}\Delta}}\right). \quad (13)$$

The spin probability rephases for $\tau=\pi/\omega_\gamma$, where $\lambda_\tau=1$, due to a perfect overlap of the states of the two branches, reduced only by NV spin decoherence with the realistic dephasing time of $T_2=10$ μs [87–89]. Other environmental decoherence channels remain negligible in the regime considered (see Supplemental Material [65]). This can be seen in Fig. 3(b), which demonstrates that increasing the rotation frequency ω enhances the interference signal by reducing the total interferometer time. Figure 3(c) shows the total interferometer time and the recurrence probability $P_\uparrow(\tau=\pi/\omega_\gamma)$ as a function of the spin-rotor coupling $g/D_{\rm nv}$. The shaded region indicates where the NV's T_2 time exceeds the interferometer time, resulting in a significant enhancement of the interference signal.

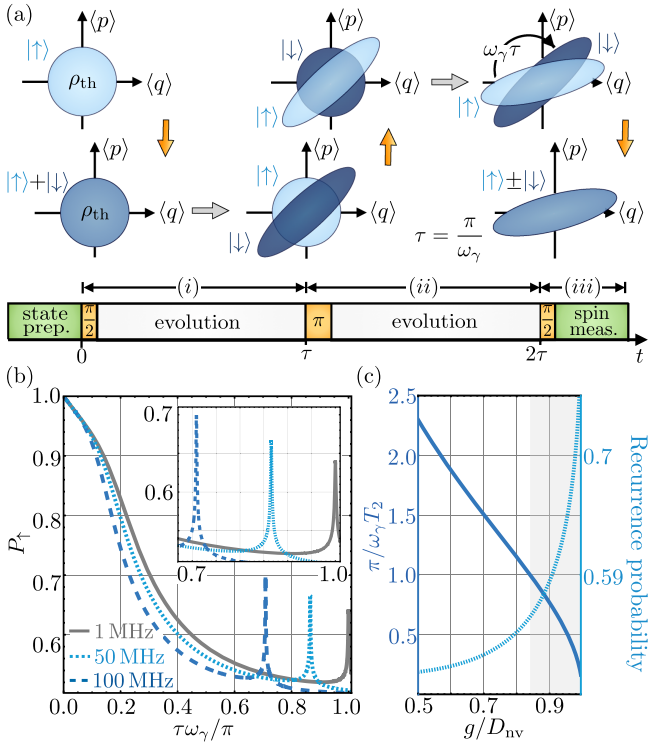


FIG. 3. (a) Pulse sequence and state evolution of the interference protocol. (b) Probability to measure $|\uparrow\rangle$ at the end of the interferometer sequence as a function of interferometer time $\tau\omega_\gamma/\pi$ (evaluated at $\omega/2\pi = 1$ MHz) for $B = -95$ mT and different rotation frequencies $\omega/2\pi = 1$ MHz (gray, solid), 50 MHz (light blue, dotted), 100 MHz (dark blue, dashed). The inset shows the probability close to rephasing. (c) Duration of the full protocol (dark blue, solid) and recurrence probability (light blue, dotted) depending on g/D_{nv}. The shaded region indicates when the interferometer time is exceeded by the T_2 time of the NV spin. The nanodiamond has an ellipsoidal shape with semiaxes $l_3 = 100$ nm and $l_1 = l_2 = 0.2l_3$.

The proposed experiments for gyroscopically stabilized spin rotors are within reach given the recent achievements in the field of levitated particles [17–19,32,48,64]. Electrically charged nanodiamonds hosting NV centers have been trapped, manipulated, and monitored both via light scattering as well as by preparation and measurements of the embedded spins (state initialization with a green laser and microwave driving to the magnetic states [90]) [31,47,91]. Gyroscopic spinning of charged particles with embedded spin degrees of freedom was recently demonstrated [32,64], achieving MHz rotation rates. Illuminating the particle with circularly polarized light can further boost the rotation rate beyond GHz [92–94].

In summary, we discussed the gyroscopic stabilization of rapidly spinning nanodiamonds with a single embedded NV spin, leading to an effective spin-rotor Hamiltonian containing only a single rotational degree of freedom. We proposed several schemes to use this Hamiltonian to probe spin-rotation coupling in state-of-the-art setups and to perform mechanical quantum interference experiments. Our Letter presents the first steps toward applications of gyroscopically stabilized spin rotors.

Acknowledgments—We thank Cosimo C. Rusconi, Sanchar Sharma, Maxime Perdriat, Julen Pedernales, and Klaus Hornberger for stimulating discussions and comments on the manuscript. V. W. and B. A. S. acknowledge funding by the Carl-Zeiss-Foundation through Project QPhoton. V. W. acknowledges support by the Deutsche Forschungsgemeinschaft (DFG, German Research Foundation) via the Research Training Group 1995 "Quantum Many-Body Methods in Condensed Matter Systems" Project No. 240766775. V. W. and S. V. K. are supported by the German Federal Ministry of Research, Technology and Space (BMFTR) Project QECHQS under Grant No. 16KIS1590K. B. A. S. is supported by the DFG No. 510794108.

Data availability—The data that support the findings of this letter are not publicly available. The data are available from the authors upon reasonable request.

[1] J. H. Van Vleck, The coupling of angular momentum vectors in molecules, Rev. Mod. Phys. **23**, 213 (1951).
[2] P. R. Bunker and P. Jensen, *Molecular Symmetry and Spectroscopy* (NRC Research Press, Ottawa, Canada, 2006).
[3] A. Einstein and W. De Haas, Experimental proof of the existence of Ampère's molecular currents, Proc. KNAW, **181**, 696 (1915).
[4] S. J. Barnett, Magnetization by rotation, Phys. Rev. **6**, 239 (1915).
[5] V. Y. Frenkel, On the history of the Einstein–de Haas effect, Sov. Phys. Usp. **22**, 580 (1979).
[6] M. Ganzhorn, S. Klyatskaya, M. Ruben, and W. Wernsdorfer, Quantum Einstein-de Haas effect, Nat. Commun. **7**, 11443 (2016).
[7] C. Dornes, Y. Acremann, M. Savoini, M. Kubli, M. J. Neugebauer, E. Abreu, L. Huber, G. Lantz, C. A. Vaz, H. Lemke *et al.*, The ultrafast Einstein–de Haas effect, Nature (London) **565**, 209 (2019).
[8] E. M. Chudnovsky, Conservation of angular momentum in the problem of tunneling of the magnetic moment, Phys. Rev. Lett. **72**, 3433 (1994).
[9] D. F. Jackson Kimball, A. O. Sushkov, and D. Budker, Precessing ferromagnetic needle magnetometer, Phys. Rev. Lett. **116**, 190801 (2016).
[10] C. C. Rusconi, V. Pöchhacker, K. Kustura, J. I. Cirac, and O. Romero-Isart, Quantum spin stabilized magnetic levitation, Phys. Rev. Lett. **119**, 167202 (2017).
[11] Y. Ma, M. Kim, and B. A. Stickler, Torque-free manipulation of nanoparticle rotations via embedded spins, Phys. Rev. B **104**, 134310 (2021).
[12] C. C. Rusconi, M. Perdriat, G. Hétet, O. Romero-Isart, and B. A. Stickler, Spin-controlled quantum interference of levitated nanorotors, Phys. Rev. Lett. **129**, 093605 (2022).

[13] K. Kustura, V. Wachter, A. E. Rubio López, and C. C. Rusconi, Stability of a magnetically levitated nanomagnet in vacuum: Effects of gas and magnetization damping, Phys. Rev. B **105**, 174439 (2022).
[14] C. Gonzalez-Ballestero, M. Aspelmeyer, L. Novotny, R. Quidant, and O. Romero-Isart, Levitodynamics: Levitation and control of microscopic objects in vacuum, Science **374**, eabg3027 (2021).
[15] D. C. Moore and A. A. Geraci, Searching for new physics using optically levitated sensors, Quantum Sci. Technol. **6**, 014008 (2021).
[16] B. A. Stickler, K. Hornberger, and M. Kim, Quantum rotations of nanoparticles, Nat. Rev. Phys. **3**, 589 (2021).
[17] U. Delić, M. Reisenbauer, K. Dare, D. Grass, V. Vuletić, N. Kiesel, and M. Aspelmeyer, Cooling of a levitated nanoparticle to the motional quantum ground state, Science **367**, 892 (2020).
[18] F. Tebbenjohanns, M. L. Mattana, M. Rossi, M. Frimmer, and L. Novotny, Quantum control of a nanoparticle optically levitated in cryogenic free space, Nature (London) **595**, 378 (2021).
[19] L. Magrini, P. Rosenzweig, C. Bach, A. Deutschmann-Olek, S. G. Hofer, S. Hong, N. Kiesel, A. Kugi, and M. Aspelmeyer, Real-time optimal quantum control of mechanical motion at room temperature, Nature (London) **595**, 373 (2021).
[20] M. Kamba, H. Kiuchi, T. Yotsuya, and K. Aikawa, Recoil-limited feedback cooling of single nanoparticles near the ground state in an optical lattice, Phys. Rev. A **103**, L051701 (2021).
[21] A. Pontin, H. Fu, M. Toroš, T. S. Monteiro, and P. F. Barker, Simultaneous cavity cooling of all six degrees of freedom of a levitated nanoparticle, Nat. Phys. **19**, 1003 (2023).
[22] L. Dania, O. S. Kremer, J. Piotrowski, D. Candoli, J. Vijayan, O. Romero-Isart, C. Gonzalez-Ballestero, L. Novotny, and M. Frimmer, High-purity quantum optomechanics at room temperature, Nat. Phys. **21**, 1603 (2025).
[23] S. Troyer, F. Fechtel, L. Hummer, H. Rudolph, B. A. Stickler, U. Delić, and M. Arndt, Quantum ground-state cooling of two librational modes of a nanorotor, arXiv:2509.13398.
[24] J. Bateman, S. Nimmrichter, K. Hornberger, and H. Ulbricht, Near-field interferometry of a free-falling nanoparticle from a point-like source, Nat. Commun. **5**, 4788 (2014).
[25] M. Roda-Llordes, A. Riera-Campeny, D. Candoli, P. T. Grochowski, and O. Romero-Isart, Macroscopic quantum superpositions via dynamics in a wide double-well potential, Phys. Rev. Lett. **132**, 023601 (2024).
[26] B. A. Stickler, B. Papendell, S. Kuhn, B. Schrinski, J. Millen, M. Arndt, and K. Hornberger, Probing macroscopic quantum superpositions with nanorotors, New J. Phys. **20**, 122001 (2018).
[27] C. Wan, M. Scala, G. Morley, A. A. Rahman, H. Ulbricht, J. Bateman, P. Barker, S. Bose, and M. Kim, Free nano-object Ramsey interferometry for large quantum superpositions, Phys. Rev. Lett. **117**, 143003 (2016).
[28] C. Wan, M. Scala, S. Bose, A. Frangeskou, A. A. Rahman, G. Morley, P. Barker, and M. Kim, Tolerance in the Ramsey interference of a trapped nanodiamond, Phys. Rev. A **93**, 043852 (2016).
[29] O. Romero-Isart, M. L. Juan, R. Quidant, and J. I. Cirac, Toward quantum superposition of living organisms, New J. Phys. **12**, 033015 (2010).
[30] M. Perdriat, C. Pellet-Mary, P. Huillery, L. Rondin, and G. Hétet, Spin-mechanics with nitrogen-vacancy centers and trapped particles, Micromachines **12**, 651 (2021).
[31] T. Delord, L. Nicolas, Y. Chassagneux, and G. Hétet, Strong coupling between a single nitrogen-vacancy spin and the rotational mode of diamonds levitating in an ion trap, Phys. Rev. A **96**, 063810 (2017).
[32] Y. Jin, K. Shen, P. Ju, X. Gao, C. Zu, A. J. Grine, and T. Li, Quantum control and Berry phase of electron spins in rotating levitated diamonds in high vacuum, Nat. Commun. **15**, 5063 (2024).
[33] M. Gutierrez Latorre, G. Higgins, A. Paradkar, T. Bauch, and W. Wieczorek, Superconducting microsphere magnetically levitated in an anharmonic potential with integrated magnetic readout, Phys. Rev. Appl. **19**, 054047 (2023).
[34] J. Hofer, R. Gross, G. Higgins, H. Huebl, O. F. Kieler, R. Kleiner, D. Koelle, P. Schmidt, J. A. Slater, M. Trupke *et al.*, High-Q magnetic levitation and control of superconducting microspheres at millikelvin temperatures, Phys. Rev. Lett. **131**, 043603 (2023).
[35] M. Fuwa, R. Sakagami, and T. Tamegai, Ferromagnetic levitation and harmonic trapping of a milligram-scale yttrium iron garnet sphere, Phys. Rev. A **108**, 063511 (2023).
[36] T. Seberson, J. Ahn, J. Bang, T. Li, and F. Robicheaux, Optical levitation of a YIG nanoparticle and simulation of sympathetic cooling via coupling to a cold atomic gas, arXiv:1910.05371.
[37] S. Chakraborty, G. K. Wong, F. Oda, V. Wachter, S. V. Kusminskiy, T. Yokosawa, S. Hübner, B. A. Zubiri, E. Spiecker, M. Distaso, P. S. J. Russell, and N. Joly, Optomagnetic forces on YIG/YFeO3 microspheres levitated in chiral hollow-core photonic crystal fibre, arXiv:2404.16182.
[38] J. Gieseler, A. Kabcenell, E. Rosenfeld, J. Schaefer, A. Safira, M. J. Schuetz, C. Gonzalez-Ballestero, C. C. Rusconi, O. Romero-Isart, and M. D. Lukin, Single-spin magnetomechanics with levitated micromagnets, Phys. Rev. Lett. **124**, 163604 (2020).
[39] F. Ahrens, W. Ji, D. Budker, C. Timberlake, H. Ulbricht, and A. Vinante, Levitated ferromagnetic magnetometer with energy resolution well below $\hbar$, Phys. Rev. Lett. **134**, 110801 (2025).
[40] J. K. Jose, A. Marchese, M. Cromb, H. Ulbricht, A. Cebers, P. K. Lam, T. Wang, and A. Vinante, Cryogenic pressure sensing with an ultrafast Meissner-levitated microrotor, arXiv:2509.24964.
[41] C. Gonzalez-Ballestero, J. Gieseler, and O. Romero-Isart, Quantum acoustomechanics with a micromagnet, Phys. Rev. Lett. **124**, 093602 (2020).
[42] V. Wachter, V. A. Bittencourt, S. Xie, S. Sharma, N. Joly, P. S. J. Russell, F. Marquardt, and S. Viola Kusminskiy, Optical signatures of the coupled spin-mechanics of a

levitated magnetic microparticle, J. Opt. Soc. Am. B **38**, 3858 (2021).
[43] A. Kani, F. Quijandría, and J. Twamley, Magnonic Einstein–de Haas effect: Ultrafast rotation of magnonic microspheres, Phys. Rev. Lett. **129**, 257201 (2022).
[44] K. Streltsov, J. S. Pedernales, and M. B. Plenio, Ground-state cooling of levitated magnets in low-frequency traps, Phys. Rev. Lett. **126**, 193602 (2021).
[45] M. O. Steiner, J. S. Pedernales, and M. B. Plenio, Pentacene-doped naphthalene for levitated optomechanics, Quantum **9**, 1928 (2025).
[46] F. Ahrens and A. Vinante, Observation of gyroscopic coupling in a non-spinning levitated ferromagnet, arXiv:2504.13744.
[47] T. Delord, P. Huillery, L. Schwab, L. Nicolas, L. Lecordier, and G. Hétet, Ramsey interferences and spin echoes from electron spins inside a levitating macroscopic particle, Phys. Rev. Lett. **121**, 053602 (2018).
[48] T. Delord, P. Huillery, L. Nicolas, and G. Hétet, Spin-cooling of the motion of a trapped diamond, Nature (London) **580**, 56 (2020).
[49] M. Geiselmann, M. L. Juan, J. Renger, J. M. Say, L. J. Brown, F. J. G. De Abajo, F. Koppens, and R. Quidant, Three-dimensional optical manipulation of a single electron spin, Nat. Nanotechnol. **8**, 175 (2013).
[50] G. P. Conangla, A. W. Schell, R. A. Rica, and R. Quidant, Motion control and optical interrogation of a levitating single nitrogen vacancy in vacuum, Nano Lett. **18**, 3956 (2018).
[51] O. Feldman, B. B. Shultz, M. Muretova, O. Dobkowski, Y. Japha, D. Grosswasser, and R. Folman, Trapping and cooling of nanodiamonds in a Paul trap under ultra-high vacuum: Towards matter-wave interferometry with massive objects, arXiv:2508.14687.
[52] M. Muretova, Y. Japha, M. Toros, and R. Folman, Parametric feedback cooling of librations of a nanodiamond in a Paul trap: Towards matter-wave interferometry with massive objects, arXiv:2508.13723.
[53] W.-L. Li and D.-L. Zhou, Preparing highly entangled states of nanodiamond rotation and NV center spin, Chin. Phys. B **33**, 020305 (2024).
[54] H. Espinós, C. Munuera-Javaloy, I. Panadero, P. Acedo, R. Puebla, J. Casanova, and E. Torrontegui, Enhancing polarization transfer from nitrogen-vacancy centers to external nuclear spins via dangling bond mediators, Commun. Phys. **7**, 42 (2024).
[55] P. Kumar and M. Bhattacharya, Magnetometry via spin-mechanical coupling in levitated optomechanics, Opt. Express **25**, 19568 (2017).
[56] X. Ni, Z. Zou, R. Lecamwasam, A. Vinante, D. Budker, P. K. Lam, T. Wang, and J. Gong, Microscopic theory of a precessing ferromagnet for ultrasensitive magnetometry, Phys. Rev. Res. **7**, 043120 (2025).
[57] S. Kalia, D. Budker, D. F. J. Kimball, W. Ji, Z. Liu, A. O. Sushkov, C. Timberlake, H. Ulbricht, A. Vinante, and T. Wang, Ultralight dark matter detection with levitated ferromagnets, Phys. Rev. D **110**, 115029 (2024).
[58] Z.-q. Yin, T. Li, X. Zhang, and L. Duan, Large quantum superpositions of a levitated nanodiamond through spin-optomechanical coupling, Phys. Rev. A **88**, 033614 (2013).
[59] J. S. Pedernales, G. W. Morley, and M. B. Plenio, Motional dynamical decoupling for interferometry with macroscopic particles, Phys. Rev. Lett. **125**, 023602 (2020).
[60] Y. Japha and R. Folman, Quantum uncertainty limit for Stern-Gerlach interferometry with massive objects, Phys. Rev. Lett. **130**, 113602 (2023).
[61] T. Zhou, S. Bose, and A. Mazumdar, Gyroscopic stability for nanoparticles in Stern-Gerlach interferometry and spin contrast, Phys. Rev. A **112**, 013315 (2025).
[62] R. Rizaldy, T. Zhou, S. Bose, and A. Mazumdar, Rotational stability in nanorotor and spin contrast in one-loop interferometry in the Stern-Gerlach setup, Phys. Rev. Res. **7**, 043095 (2025).
[63] S. Bose, A. Mazumdar, G. W. Morley, H. Ulbricht, M. Toroš, M. Paternostro, A. A. Geraci, P. F. Barker, M. Kim, and G. Milburn, Spin entanglement witness for quantum gravity, Phys. Rev. Lett. **119**, 240401 (2017).
[64] M. Perdriat, C. C. Rusconi, T. Delord, P. Huillery, C. Pellet-Mary, A. Durand, B. A. Stickler, and G. Hétet, Rotational locking of charged microparticles in quadrupole ion traps, Phys. Rev. Lett. **133**, 253602 (2024).
[65] See Supplemental Material at http://link.aps.org/supplemental/10.1103/zjpt-whpf for derivations and supporting information, which includes Refs. [66–82].
[66] C. C. Rusconi and O. Romero-Isart, Magnetic rigid rotor in the quantum regime: Theoretical toolbox, Phys. Rev. B **93**, 054427 (2016).
[67] M. Ban, SU(1,1) Lie algebraic approach to linear dissipative processes in quantum optics, J. Math. Phys. (N.Y.) **33**, 3213 (1992).
[68] J. Achard, V. Jacques, and A. Tallaire, Chemical vapour deposition diamond single crystals with nitrogen-vacancy centres: A review of material synthesis and technology for quantum sensing applications, J. Phys. D **53**, 313001 (2020).
[69] Y.-C. Chen, P. S. Salter, S. Knauer, L. Weng, A. C. Frangeskou, C. J. Stephen, S. N. Ishmael, P. R. Dolan, S. Johnson, B. L. Green *et al.*, Laser writing of coherent colour centres in diamond, Nat. Photonics **11**, 77 (2017).
[70] K. Kinouchi, Y. Shimotsuma, M. Uemoto, M. Fujiwara, N. Mizuochi, M. Shimizu, and K. Miura, Laser writing of preferentially orientated nitrogen-vacancy centers in diamond, Carbon Trends **13**, 100318 (2023).
[71] F. Monteiro, S. Ghosh, E. C. van Assendelft, and D. C. Moore, Optical rotation of levitated spheres in high vacuum, Phys. Rev. A **97**, 051802 (2018).
[72] T. Seberson and F. Robicheaux, Parametric feedback cooling of rigid body nanodumbbells in levitated optomechanics, Phys. Rev. A **99**, 013821 (2019).
[73] D. Kim, S. Tian, B. Calderoni, C. S. Jachimska, J. Downes, and J. Twamley, A magnetically levitated conducting rotor with ultra-low rotational damping circumventing eddy loss, Commun. Phys. **8**, 381 (2025).
[74] L. Martinetz, K. Hornberger, and B. A. Stickler, Gas-induced friction and diffusion of rigid rotors, Phys. Rev. E **97**, 052112 (2018).
[75] L. Martinetz, Quantum electromechanics with levitated charged particles, Ph.D. thesis, Dissertation, Duisburg, Essen,

Universität Duisburg-Essen, 2023, https://duepublico2.uni-due.de/receive/duepublico_mods_00078558.
[76] L. Martinetz, K. Hornberger, and B. A. Stickler, Surface-induced decoherence and heating of charged particles, PRX Quantum **3**, 030327 (2022).
[77] N. Glikin, B. A. Stickler, R. Tollefsen, S. Mouradian, N. Yadav, E. Urban, K. Hornberger, and H. Häffner, Probing rotational decoherence with a trapped-ion planar rotor, Phys. Rev. Lett. **134**, 033601 (2025).
[78] M. W. Mitchell and S. Palacios Alvarez, Colloquium: Quantum limits to the energy resolution of magnetic field sensors, Rev. Mod. Phys. **92**, 021001 (2020).
[79] B. Papendell, B. A. Stickler, and K. Hornberger, Quantum angular momentum diffusion of rigid bodies, New J. Phys. **19**, 122001 (2017).
[80] J. Schäfer, B. A. Stickler, and K. Hornberger, Decoherence of dielectric particles by thermal emission, Phys. Rev. Res. **6**, 043307 (2024).
[81] M. W. Doherty, F. Dolde, H. Fedder, F. Jelezko, J. Wrachtrup, N. B. Manson, and L. C. L. Hollenberg, Theory of the ground-state spin of the NV^- center in diamond, Phys. Rev. B **85**, 205203 (2012).
[82] F. Dolde, H. Fedder, M. W. Doherty, T. Nöbauer, F. Rempp, G. Balasubramanian, T. Wolf, F. Reinhard, L. C. Hollenberg, F. Jelezko *et al.*, Electric-field sensing using single diamond spins, Nat. Phys. **7**, 459 (2011).
[83] L. Martinetz, K. Hornberger, and B. A. Stickler, Electric trapping and circuit cooling of charged nanorotors, New J. Phys. **23**, 093001 (2021).
[84] H. Chudo, K. Harii, M. Matsuo, J. Ieda, M. Ono, S. Maekawa, and E. Saitoh, Rotational Doppler effect and Barnett field in spinning NMR, J. Phys. Soc. Jpn. **84**, 043601 (2015).
[85] A. A. Wood, E. Lilette, Y. Y. Fein, N. Tomek, L. P. McGuinness, L. C. Hollenberg, R. E. Scholten, and A. M. Martin, Quantum measurement of a rapidly rotating spin qubit in diamond, Sci. Adv. **4**, eaar7691 (2018).
[86] A. A. Wood, L. C. Hollenberg, R. E. Scholten, and A. M. Martin, Observation of a quantum phase from classical rotation of a single spin, Phys. Rev. Lett. **124**, 020401 (2020).
[87] J. F. Barry, J. M. Schloss, E. Bauch, M. J. Turner, C. A. Hart, L. M. Pham, and R. L. Walsworth, Sensitivity optimization for NV-diamond magnetometry, Rev. Mod. Phys. **92**, 015004 (2020).
[88] X.-Y. Chen, C.-D. Qiu, Y.-N. Lu, G.-Q. Liu, D. Ruan, F. Zhang, and G. Long, Extending dephasing time of nitrogen-vacancy center in diamond by suppressing nuclear spin noise, Phys. Rev. B **108**, 174111 (2023).
[89] J. Du, F. Shi, X. Kong, F. Jelezko, and J. Wrachtrup, Single-molecule scale magnetic resonance spectroscopy using quantum diamond sensors, Rev. Mod. Phys. **96**, 025001 (2024).
[90] T. F. Segawa and R. Igarashi, Nanoscale quantum sensing with nitrogen-vacancy centers in nanodiamonds–a magnetic resonance perspective, Prog. Nucl. Magn. Reson. Spectrosc. **134**, 20 (2023).
[91] T. M. Hoang, J. Ahn, J. Bang, and T. Li, Electron spin control of optically levitated nanodiamonds in vacuum, Nat. Commun. **7**, 12250 (2016).
[92] R. Reimann, M. Doderer, E. Hebestreit, R. Diehl, M. Frimmer, D. Windey, F. Tebbenjohanns, and L. Novotny, GHz rotation of an optically trapped nanoparticle in vacuum, Phys. Rev. Lett. **121**, 033602 (2018).
[93] J. Ahn, Z. Xu, J. Bang, Y.-H. Deng, T. M. Hoang, Q. Han, R.-M. Ma, and T. Li, Optically levitated nanodumbbell torsion balance and GHz nanomechanical rotor, Phys. Rev. Lett. **121**, 033603 (2018).
[94] Y. Jin, J. Yan, S. J. Rahman, J. Li, X. Yu, and J. Zhang, 6 GHz hyperfast rotation of an optically levitated nanoparticle in vacuum, Photonics Res. **9**, 1344 (2021).